Determining the atomic charge of calcium ion requires the information of its coordination geometry in an EF-hand motif

(iD) **Pengzhi Zhang,** (iD) **Jaebeom Han,** (iD) **Piotr Cieplak, and** (iD) **Margaret. S. Cheung**

COLLECTIONS

Paper published as part of the special topic on Special Collection in Honor of Women in Chemical Physics and Physical Chemistry

View Online   Export Citation   CrossMark

ARTICLES YOU MAY BE INTERESTED IN

A practical guide to biologically relevant molecular simulations with charge scaling for electronic polarization
The Journal of Chemical Physics **153**, 050901 (2020); https://doi.org/10.1063/5.0017775

Improving molecular force fields across configurational space by combining supervised and unsupervised machine learning
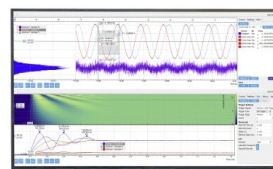The Journal of Chemical Physics **154**, 124102 (2021); https://doi.org/10.1063/5.0035530

Classical molecular dynamics
The Journal of Chemical Physics **154**, 100401 (2021); https://doi.org/10.1063/5.0045455

Determining the atomic charge of calcium ion requires the information of its coordination geometry in an EF-hand motif

View Online   Export Citation   CrossMark

Pengzhi Zhang,[1] (iD) Jaebeom Han,[1] (iD) Piotr Cieplak,[2] (iD) and Margaret. S. Cheung[1,3,a] (iD)

AFFILIATIONS

[1] Department of Physics, University of Houston, Houston, Texas 77204, USA
[2] Sanford Burnham Prebys Medical Discovery Institute, La Jolla, California 92037, USA
[3] Center for Theoretical Biological Physics, Rice University, Houston, Texas 77005, USA

Note: This paper is part of the JCP Special Collection in Honor of Women in Chemical Physics and Physical Chemistry.
[a] Author to whom correspondence should be addressed: mscheung@uh.edu

ABSTRACT

It is challenging to parameterize the force field for calcium ions (Ca^{2+}) in calcium-binding proteins because of their unique coordination chemistry that involves the surrounding atoms required for stability. In this work, we observed a wide variation in Ca^{2+} binding loop conformations of the Ca^{2+}-binding protein calmodulin, which adopts the most populated ternary structures determined from the molecular dynamics simulations, followed by *ab initio* quantum mechanical (QM) calculations on all 12 amino acids in the loop that coordinate Ca^{2+} in aqueous solution. Ca^{2+} charges were derived by fitting to the electrostatic potential in the context of a classical or polarizable force field (PFF). We discovered that the atomic radius of Ca^{2+} in conventional force fields is too large for the QM calculation to capture the variation in the coordination geometry of Ca^{2+} in its ionic form, leading to unphysical charges. Specifically, we found that the fitted atomic charges of Ca^{2+} in the context of PFF depend on the coordinating geometry of electronegative atoms from the amino acids in the loop. Although nearby water molecules do not influence the atomic charge of Ca^{2+}, they are crucial for compensating for the coordination of Ca^{2+} due to the conformational flexibility in the EF-hand loop. Our method advances the development of force fields for metal ions and protein binding sites in dynamic environments.

I. INTRODUCTION

Calcium ions (Ca^{2+}) are a key second messenger controlling many biological processes, such as enzyme activation, muscle contraction, and neural signal transduction. A broad spectrum of Ca^{2+} signals are encoded by the protein calmodulin (CaM) through specific binding with various targets that regulate CaM-dependent Ca^{2+} signaling pathways in neurons.[1–3] CaM can bind up to four Ca^{2+} ions through its four helix–coil–helix (called EF-hand) structures.[4] In the coil connecting the two helices, termed the EF-hand loop, there are usually six residues that cooperatively coordinate Ca^{2+} to form a pentagonal bipyramidal geometry [Figs. 1(a) and 1(b)]. Binding of Ca^{2+} in the EF-hand structure widens the angle between the two helices, as seen in the right inter-helical angle in

Fig. 1(a). Although the four Ca^{2+} binding loops present similar helix–coil–helix structures, they show dissimilar capacities of retaining Ca^{2+}. The two loops in the N-lobe of CaM (nCaM) bind Ca^{2+} faster than those in the C-lobe of CaM (cCaM), and Ca^{2+} dissociates faster from nCaM than from cCaM.[5] The reasons are elusive and lie in the subtle difference in the amino acid sequences of the four EF-hand loops and the mobility of the water molecules packed in the loops (Table I).

The conformation of the calcium binding loop in CaM is finely tuned by CaM-binding proteins,[6] which underscores the reciprocal relationship of transmitting calcium signals to target selection regulating downstream proteins, and vice versa, in a CaM-depending calcium signaling pathway. Such an aspect has been underappreciated in the community of molecular dynamics (MD) simulations
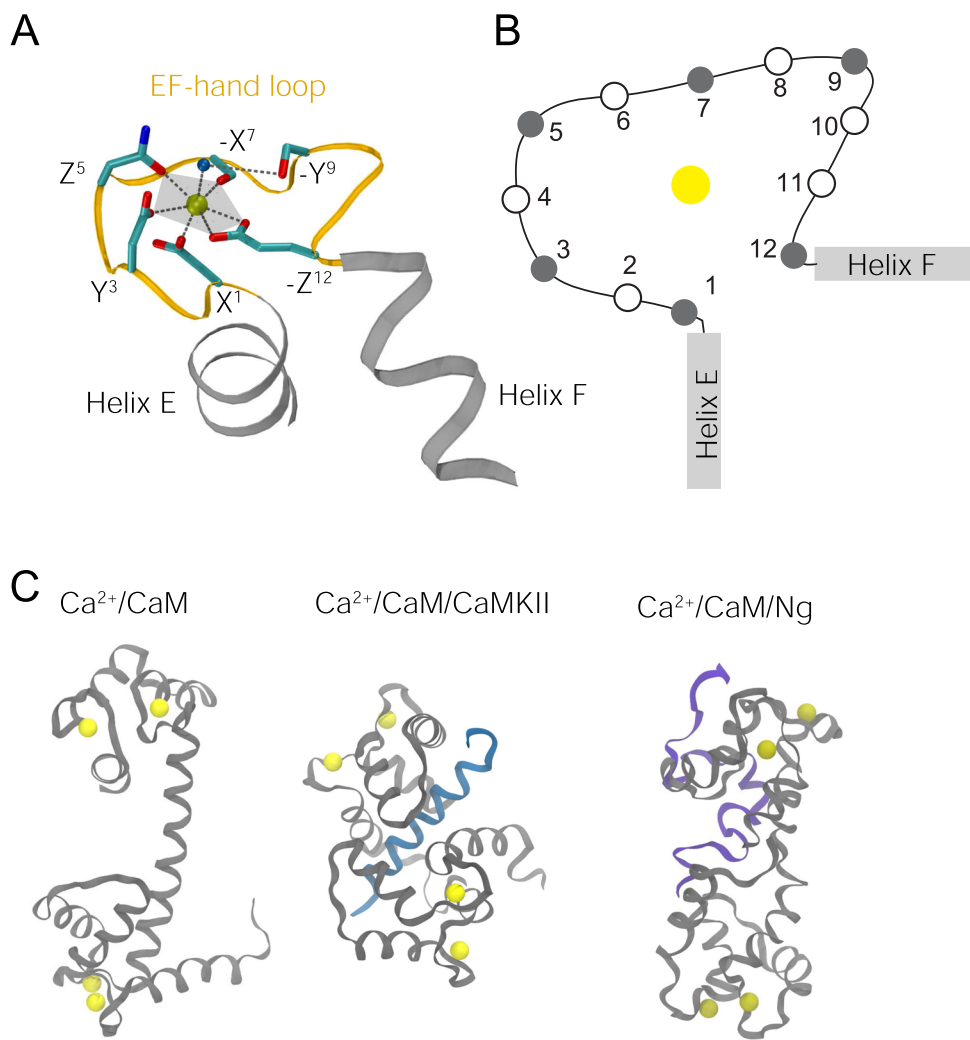
FIG. 1. Coordination of Ca^{2+} in the EF-hand loops: (a) The coordination geometry in EF-hand 3 from the crystal structure of Ca^{2+}/CaM (PDB ID: 1CLL). An EF-hand is made up of helix E (gray), EF-hand loop (orange), and helix F (gray). The Ca^{2+} ion is represented by a yellow bead. Side chains of the Ca^{2+}-coordinating residues in the EF-hand loop are represented by sticks (coloring: red → oxygen; cyan → carbon; blue → nitrogen). The oxygen atom of the bridging water molecule is represented as a blue bead. The coordination positions of the Ca^{2+} ion are denoted ($\pm$X, $\pm$Y, and $\pm$Z). (b) Schematic illustration of the positions of the residues in an EF-hand loop. The filled circles are the ones that coordinate Ca^{2+} (Table I). (c) Illustration of the structures of Ca^{2+}/CaM (PDB ID: 1CLL), the Ca^{2+}/CaM/CaMKII peptide (PDB ID: 1CDM), and the Ca^{2+}/CaM/Ng peptide (reconstructed from previous coarse-grained simulations, as described in Sec. II A). Ca^{2+} is in yellow, CaM is in gray, the CaMKII peptide is in blue, and the Ng peptide is in purple. Abbreviations: CaMKII (Ca^{2+}/CaM-dependent protein kinase II); Ng (neurogranin).

with di-valent ions, where the charges of divalent ions are typically fixed in a mean-field approach.

MD simulations are an excellent tool to investigate the subtle difference in the calcium binding affinities in the four EF-hand loops of CaM. However, there is a lack of adequate force fields including adequate polarization effects for Ca^{2+} in Ca^{2+}-binding proteins due to several major limitations. First, developing more accurate MD force fields (MDFFs) for Ca^{2+} and its binding component usually

TABLE I. Amino acid sequences of the four Ca^{2+} binding loops (EF-1, EF-2, EF-3, and EF-4) in calmodulin. Their coordination positions for Ca^{2+} ions are also provided. # denotes the residue that coordinates Ca^{2+} ions through backbone oxygen. $*$ denotes the residue that indirectly coordinates Ca^{2+} through a water molecule.

Residue index		1	2	3	4	5	6	7	8	9	10	11	12
Coordination position		X		Y		Z		$-$Y$^{\#}$		$-$X*			$-$Z
nCaM	EF-1	D	K	D	G	D	G	T	I	T	T	K	E
	EF-2	D	A	D	G	N	G	T	I	D	F	P	E
cCaM	EF-3	D	K	D	G	N	G	Y	I	S	A	A	E
	EF-4	D	I	D	G	D	G	Q	V	N	Y	E	E

requires a series of computationally demanding quantum mechanical (QM) calculations to provide electronic structures whose computational cost increases quartically with the system size.[7] Second, when mapping the electronic structures to a point charge in MDFFs in exchange for speed in MD simulations, the interaction between a divalent ion and its receptor protein is simplified and devoid of strong polarization as well as charge-transfer effects.[8–12] Third, the Ca^{2+}-binding component in the protein, due to structural flexibility in both the backbone and side chains, usually generates a myriad of ensemble conformations, further increasing the computational cost associated with collecting more configurations in an attempt to attain statistical significance by minimizing sampling errors.[13] Even when the many-body polarization effect has been included in Ren's *ab initio* calculations,[11] the heavy calculation was based on single structure for a protein without the consideration of the thermodynamic effect.

In a crystal structure of the EF-hand loop, Ca^{2+} is coordinated in a pentagonal bipyramidal coordination geometry (Fig. 1), where Ca^{2+} is coordinated not only by carboxylate oxygen atoms from the side chains but also by one carbonyl oxygen atom from the backbone and the oxygen atoms from water molecules (one typical example is in the crystal structure of Ca^{2+}/CaM, as shown in Table I). The coordination geometry is vital in stabilizing the ion.[14–16] To address the many-body polarization effect[11] and taking the loop flexibility into account, we derived the charges of Ca^{2+} using *ab initio* quantum calculations of the Ca^{2+} embedded in EF-hand loops (including coordinating water molecules) in several hundred distinct conformations. These loop conformations were based on CaM in Ca^{2+}-retaining/Ca^{2+}-releasing environments from the existing solved structures or all-atomistic models reconstructed from our prior work.[8] The structural flexibility in the Ca^{2+}-binding protein can cause the change in the Ca^{2+}-coordinating atoms and charge transfer between Ca^{2+} and protein. We show that the derived Ca^{2+} charges and the charges on the protein change with the varying loop conformations. We have concluded that because of the variation in the Ca^{2+} charge, one set of parameters are not suitable to study the dynamics of Ca^{2+}-protein interaction. Our method/workflow can be easily applied to other Ca^{2+} binding environments and other di-valent ions[17,18] such as Mg^{2+} in cases when the coordination geometry of the cation dynamically adapts to the environment.

II. MATERIALS AND METHODOLOGY

The atomic partial charge is built on the existing nonpolarizable force field (NFF)[19,20] or polarizable force field (PFF) methodology[21–26] taking polarization interactions into consideration. The steps to determine the atomic charges are shown in Fig. 2. The parameters of NFF and PFF have been derived using a broad collection of Ca^{2+}-binding loops from all-atomistic MD simulations in an explicit solvent for an isolated CaM (Ca^{2+}/CaM) or its bound complexes from an available database. This approach warrants a broad coverage of the configuration space of Ca^{2+} and the dynamics of its binding EF-hand loops involving the steps shown below in Fig. 2.

A. Sample selections for the initial conditions

Samples of Ca^{2+}/CaM from all-atom models in the following three conditions were examined. (1) Neat Ca^{2+}/CaM: the crystal
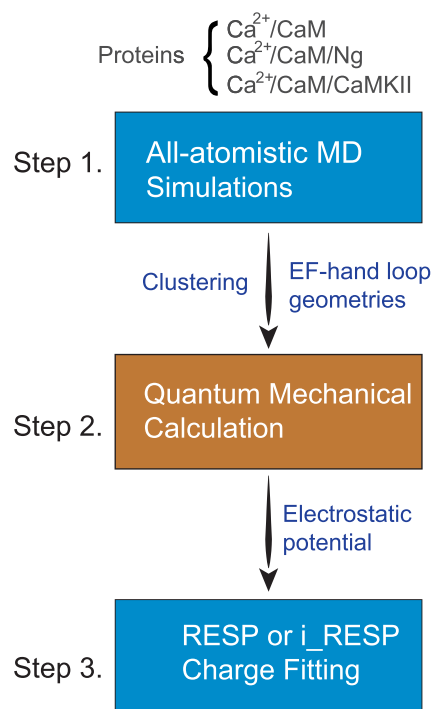

FIG. 2. Flowchart of the determination of atomic charges from MD-generated geometries using the RESP/i_RESP charge fitting method.

structure (PDB ID: 1CLL) was used as the initial structure; (2) Ca^{2+}-retaining environment consisting of the Ca^{2+}/CaM/CaM-dependent protein kinase II (CaMKII) peptide: the crystal structure (PDB ID: 1CDM, respectively) was used as the initial structure; (3) Ca^{2+}-releasing environment consisting of the Ca^{2+}/CaM/neurogranin (Ng) peptide: three representative complex structures were used as the initial structures. We reconstructed those structures into all-atomistic models from coarse-grained models with constraints inferred from the changes in the chemical shifts obtained from nuclear magnetic resonance (NMR) experiments.[6,8] The coordinates of the reconstructed all-atomistic models of Ca^{2+}/CaM/Ng are provided in the PDB format in the supplementary material.

B. Generation of the ensemble structures by molecular dynamics simulations

To generate a broad ensemble of Ca^{2+}-binding EF-hand loop geometries, all-atom MD simulations of the three systems were performed with GROMACS version 2018[27] in a periodic box of ~$10 \times 10 \times 10$ nm^3 with an explicit solvent. CaM or CaM in complex with a CaM-binding target (CaMBT; CaMBT can be CaMKII or Ng peptide) was placed at least 1 nm away from the edges of the cubic box. The system was solvated by explicit water molecules using the rigid three-site TIP3P model.[28] The lengths of bonds involving H atoms in the proteins were constrained using the LINCS

algorithm.[29] The system was neutralized by K^+ and Cl^- ions, maintaining a physiological ionic strength of 150 mM. The AMBER force field FF-99SB-ILDN[30] was adopted. Electrostatic interactions between periodic images were treated using the particle mesh Ewald (PME) approach,[31] with a grid size of 0.16 nm, fourth-order cubic interpolation, and a tolerance of 10^{-5}. Neighbor lists were updated dynamically. A cutoff of 10 Å was used for van der Waals (vdW) interactions, for real space Coulombic interactions, and for updating the neighbor lists.

For each simulated system, energy minimization was carried out with the steepest descent method to remove unfavorable clashes between atoms. Next, the system was gradually heated to 300 K in a canonical ensemble (NVT) in 1 ns, followed by 1 ns of equilibration of the solvents and ions (the proteins were constrained in their current positions) in an isothermal–isobaric ensemble (NPT) to fix the density. The constraints on the proteins were then released, and the system was further equilibrated for 5 ns. Finally, a 100 ns NPT simulation was carried out for the production run. All NPT simulations maintained a constant pressure of 1 bar using a Parrinello–Rahman barostat.[32] The equation of motion was integrated using a time step of 2 fs. Snapshots were saved for analysis every 1 ps.

In total, we generated 500 000 snapshots of Ca^{2+}/CaM from the MD simulations. With four EF-hand loops in each CaM, we generated 2×10^6 loop structures and further applied clustering analyses to extract the most dominant configurations for the QM calculations.

C. Importance sampling of Ca^{2+}/binding EF-hand geometries: Application of neural-net clustering to molecular dynamics snapshots

We applied a nonhierarchical clustering algorithm[33] to 2M snapshots of Ca^{2+}-binding loop geometries. We used normalized radial and angular distribution functions as the molecular feature[34,35] in the neural-net clustering analysis. We focus on the chemical environment surrounding Ca^{2+} by using distribution functions to remove the translational and rotational degrees of freedom. The equations and description of the distribution functions are provided in the supplementary material. A common cutoff of 0.6 was used for EF-hand loops 1–4 to generate 155, 242, 215, and 164 clusters, respectively, for further *ab initio* calculations. In addition to the selected EF-hand loops, the corresponding Ca^{2+} ions and the water molecules in the first solvation shell were extracted for the QM *ab initio* calculations.

D. *Ab initio* quantum mechanical calculations

To determine the magnitude of charge transfer between Ca^{2+} ions and the amino acids in the calcium-binding loop, we performed a large-scale *ab initio* quantum mechanical calculation in terms of both the number of atoms and the number of snapshots. *Ab initio* calculations were conducted for loop fragments including Ca^{2+} ions and water molecules in the first solvation shell of Ca^{2+}. The loop structures were capped with acetyl and methyl groups at the C- and N-termini, respectively, before performing the *ab initio* calculations. We explicitly included water molecules in the polarizable environment in the QM calculations instead of treating the solvent as a polarizable continuum. All *ab initio* calculations were performed with the Gaussian16[36] program. The molecular electrostatic

potential (ESP) derived from the electronic structures by the *ab initio* calculations was further used for fitting excess atomic charges in the context of either a nonpolarizable force field (NFF) or a polarizable force field (PFF).

E. The development of atomic charges in the nonpolarizable force field and polarizable force field

We employed the restrained electrostatic potential (RESP) and i_RESP charge fitting parameterization protocol to fit the partial atomic charges for the NFF and PFF, respectively. For PFF, the atomic charges conforming to the Thole-linear polarization model were fitted to the molecular electrostatic potentials with the i_RESP program.[37] The 1–2 and 1–3 short-range interactions were excluded from the fitting, while the 1–4 long-range interactions were included. In the fitting involving water molecules, we used atomic charges and polarizabilities from the POL3 water model.[38] For Ca^{2+} ions, we used an experimental ionic polarizability of 3.26 a.u. (0.483 Å^3).[39]

III. RESULTS

A. The B3LYP/SVP basis set balances accuracy and computational cost in *ab initio* quantum mechanical calculations

As the first attempt to run QM calculations at the MP2/aug-cc-pVTZ theory level, which was used for deriving the original AMBER Thole-linear polarization force field,[40] we set up small systems involving only three amino acid side chains (2 Asp and 1 Glu in EF-3) and Ca^{2+} ions. However, this basis set is not available for Ca^{2+} ions. We next mixed the aug-cc-pVTZ basis set for the side chain atoms with the cc-pVTZ basis set that is available for Ca^{2+} ions, but it often led to an unstable self-consistent field (SCF) process for many configurations and required a prohibitively long computation time. To stabilize the configuration by satisfying the coordination chemistry of Ca^{2+} ions, it is necessary to include all loop residues and water molecules from the first solvation shell.

However, once we increased the number of residues to include the entire calcium-binding loop in the QM calculations, the computational cost immediately became prohibitive. To make our large-scale QM calculations feasible, we applied the B3LYP-type exchange and correlation functional[41] and the split-valence polarization (SVP) basis set.[42] We validated our choice of B3LYP/SVP instead of the MP2/aug-cc-pVTZ level of theory for charge derivation by performing a series of QM calculations at both the B3LYP/SVP and MP2/aug-cc-pVTZ levels of theory for various tetrapeptides, ACE-Ala-X-Ala-NME, where X is one of the eight amino acids observed in CaM calcium binding loops, as summarized in Table I.

In the calculations, we considered five standard conformations for each tetrapeptide, namely, parallel β-sheet, antiparallel β-sheet, right-handed α-helix, left-handed α-helix, and PPII (left-handed polyproline II helical structure). The final atomic charges were fitted with the RESP and i_RESP programs (Fig. 2) for each tetrapeptide, treating either each conformation separately or jointly (joint fit
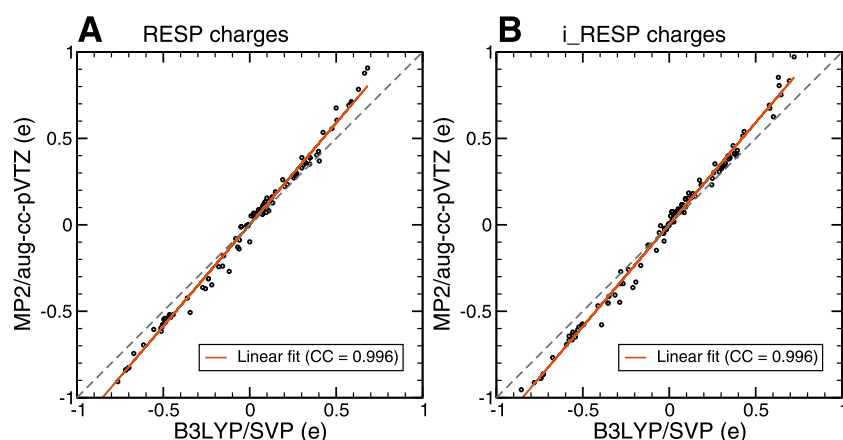
FIG. 3. Correlation between the fitted charges using electrostatic potentials (ESPs) at the B3LYP/SVP and MP2/aug-cc-pVTZ levels of theory: (a) Atomic charges were fitted using RESP. (b) Atomic charges were fitted using i_RESP. The ESPs were calculated using QM for the tetrapeptides ACE-Ala-X-Ala-NME, where X is one of the eight different amino acids observed in CaM Ca^{2+} binding loops.

across five conformations). As summarized in Table SI, the mean absolute difference (MAD) between the i_RESP atomic charges derived at the B3LYP/SVP and MP2/aug-cc-pVTZ levels of theory is small, smaller than 0.11e on average. The root mean square difference (RMSD) between the i_RESP charges at these two QM levels of theory has a similar magnitude and does not exceed 0.13e. Interestingly, both MAD and RMSD parameters are smaller (by 15%–40%) for charges obtained from the joint fit of five conformations compared to the separate fit (Table SI).

We found that regardless of which fitting method (RESP or i_RESP) was used, the atomic charges obtained from the ESPs with the two levels of theory were in strong agreement and were highly correlated (Fig. 3). Thus, the B3LYP/SVP level of theory for derivation of charges has reasonable accuracy compared to that of MP2/aug-cc-pVTZ for the systems we studied.

B. Setting up an appropriate radius for the Ca^{2+} ion is crucial to fit the accurate atomic charge

The results for the tetrapeptides showed that not only B3LYP/SVP is comparable to MP2/aug-cc-pVTZ, but it also enables us to expand the number of atoms in the QM calculations and will

enable us to determine the many-body effect with only a minor loss of precision. Furthermore, it permits the efficient computation of the electronic structures from a large ensemble of loop conformations, which improves the accuracy of the overall distribution of the atomic charges. Altogether, the calculations were performed for 776 different loop conformations and involved 173–194 atoms and 1693–1861 basis set functions.

In the calculation of the ESPs from the electronic structures of the Ca^{2+}-binding loops, we needed to manually define the vdW radius for the Ca^{2+} ions (σ_{vdW}) to build the surface grids. Initially, we set $\sigma_{vdW} = 1.7$ Å, the same as the vdW radius used in the AMBER force fields adapted from Aqvist.[43] By fitting to the obtained ESPs using the RESP or i_RESP method, we acquired the atomic charges of the Ca^{2+} ion and of the atoms in the protein. We found that unphysical values for the Ca^{2+} i_RESP charges were generated, e.g., $Q > 4e$ or $Q < 0$ [Fig. 4(a)]. More unphysical values were obtained for the protein atomic charges. Specifically, for the i_RESP charges, there was a long tail of unphysical charges $>3e$ in the Gaussian-like distribution of the Ca^{2+} atomic charges [Fig. 4(b)].

We noted that such irregularities were due to the radius of Ca^{2+}. The default radius of 1.7 Å for Ca^{2+} in the AMBER force field is
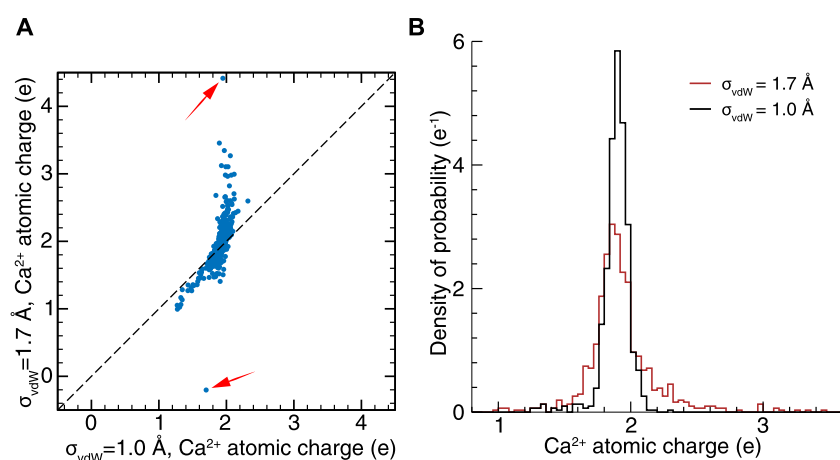

FIG. 4. Comparison between the i_RESP charges of the Ca^{2+} ion from the electrostatic potential using the vdW radii of $Ca^{2+} = 1.0$ Å and 1.7 Å. (a) Direct comparison between the two sets of i_RESP charges. The red arrows indicate excessively unphysical charges generated using $\sigma_{vdW} = 1.7$ Å. (b) Distribution of the i_RESP charges. The distribution was obtained using 776 representative EF-hand loop structures.

the vdW radius for the atomic Lennard-Jones potential of calcium, while the ionic radius of Ca^{2+} should be smaller. The ionic radius of Ca^{2+} depends on the coordination number (CN); for CN = 6, 7, and 8, σ_{vdW} was determined to be 1.00, 1.06, and 1.12 Å, respectively.[44] Therefore, we explored the dependency of the Ca^{2+} atomic charges on the ionic radii over a range of values. We compared the Ca^{2+} atomic charges derived from ESPs using σ_{vdW} = 1.00, 1.06, 1.12, and 1.70 Å using the specific structure for which the Ca^{2+} i_RESP charge was +4.4e. We show in Fig. S4 that, unlike at σ_{vdW} = 1.70 Å, the i_RESP charges of Ca^{2+} at σ_{vdW} = 1.00–1.12 Å were ~1.95e. On the other hand, the RESP charges of Ca^{2+} at σ_{vdW} = 1.00–1.12 Å were ~1.7e, which is slightly larger than that derived at σ_{vdW} = 1.70 Å (1.6e). Moreover, the calcium ion charges were insensitive to σ_{vdW} values from 1.00 to 1.12 Å. Therefore, we set the ionic radius σ_{vdW} = 1.0 Å in the calculations for all conformers of the EF-hand loops, where the CN may vary.

For the i_RESP atomic charges of Ca^{2+} for all conformers, the Gaussian-like distribution was narrower at σ_{vdW} = 1.0 Å than at σ_{vdW} = 1.7 Å. Most importantly, unphysical charges greater than +3e or less than 0 have never been observed [Fig. 4(b)]. For the RESP charges, the width of the distribution became narrower at σ_{vdW} = 1.0 Å, and the mean shifted from 1.5e to ~1.8e (Fig. S3). We showed that the use of the ionic radius (σ_{vdW} = 1.0 Å) was more appropriate than using the covalent radius for addressing Ca^{2+} molecular ESPs in Ca^{2+}-binding proteins with explicit water molecules. By using σ_{vdW} = 1.0 Å, we found that compared with the Mulliken charges or the RESP charges, the i_RESP charges present the largest mean and standard deviation values. This is because the i_RESP charges are more susceptible to the variation in the neighboring atoms by including the polarization effect. Details can be found in Fig. S1 and Text S1 of the supplementary material.

C. Nearby water molecules have no substantial effect on tuning the atomic charge of Ca^{2+}

We found that the number of water molecules that chelates Ca^{2+}, N_{water}, varies in the EF-hand loops. In the crystal structure of the EF-hand loops in CaM (PDB ID: 1CLL), there can be one crystal water molecule that chelates Ca^{2+}. In the MD simulations, the first solvation shell extended up to 3.3 Å away from the Ca^{2+} ion [see the radial distribution function $g_{Ca-O}(r)$ for Ca^{2+} and the oxygen atoms in the water molecules in Text S2 and Fig. S5 of the supplementary material]. The probability distribution of N_{water} (Fig. 5) shows that most EF-hand loops retain two water molecules. Specifically, for EF-1, in more than half of the snapshots, there are two water molecules, whereas N_{water} ranges from 4 to 6 for the others; for EF-2, N_{water} varies from 1 to 7 with similar probabilities; for EF-3 and EF-4, the probability of observing N_{water} decreases almost monotonically from 2 to 6.

N_{water} is further tuned by target-binding. In the CaM/Ng complex, N_{water} varies from 2 to 7 (Fig. S6), as the Ca^{2+} ion is not favorably retained because of the shape of the loops, which are more flexible and less spherical (Fig. 8). This effect is mainly due to the disruptive interaction between the Ng peptide and the Ca^{2+}-binding loops in CaM.

Next, we investigated the effect of water molecules on the atomic charge of Ca^{2+} ions and proteins. To determine how many water molecules are needed to derive reliable atomic charges of Ca^{2+}
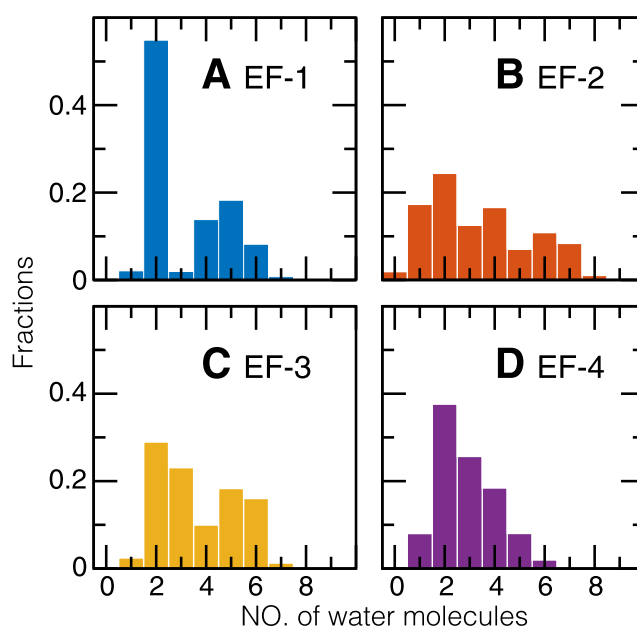

FIG. 5. Fraction of the number of water molecules in individual Ca^{2+}-binding EF-hand loops. The distributions were calculated by considering all the trajectories from all-atomistic molecular dynamics simulations of Ca^{2+}/CaM, Ca^{2+}/CaM/CaMKII, and Ca^{2+}/CaM/Ng in explicit solvents. The water molecules were counted within the first solvation shell of Ca^{2+} ions.

ions, we systematically varied the number of water molecules in the calculation from 0 to 4. As we learned that i_RESP charges are more susceptible to the environment (see Text 1 of the supplementary material), we focused on i_RESP charges here. In the fitting, we kept the original parameters of the POL3 water model, including atomic partial charges, atomic polarizabilities of O and H, and the screening factor. We selected 163 representative EF-hand loop structures from the simulation of Ca^{2+}/CaM and Ca^{2+}/CaM/CaMKII. In 152 structures, the number of water molecules in the first solvation shell varied from 1 to 4; in the remaining 11 structures, water was absent.

The average generated i_RESP charges of Ca^{2+} as a function of the number of water molecules around the ion are shown in Fig. 6. In general, the Ca^{2+} atomic charge gradually decreased with an increasing number of water molecules; however, the change in the Ca^{2+} charge was almost negligible (<1%). This indicates that although the number of water molecules surrounding Ca^{2+} in the calcium binding loop varies, water is noninfluential in determining the charge of Ca^{2+}. Therefore, we suggest including one water molecule to maintain the correct coordination chemistry of the pentagonal bipyramidal geometry in the quantum chemical calculations to determine the Ca^{2+} charge.

D. Charges are distributed unevenly in each EF-hand loop

Since water does not have a substantial role in determining the atomic charge of Ca^{2+}, we further investigated the charge
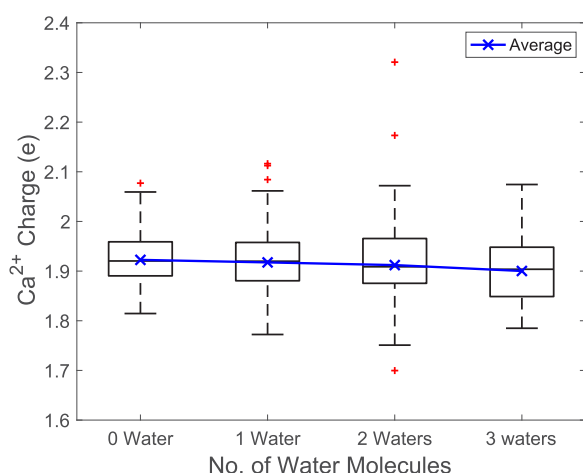
FIG. 6. Boxplot of the atomic charges of Ca^{2+} with different numbers of water molecules included in the calculation. The mean value of the Ca^{2+} charges is shown by the blue solid line. The boxplot is shown in black, and the outliers are shown in red.

distribution on the amino acids from the four EF-hand loops. In Fig. 7, we plotted the averaged i_RESP charges on each residue in the EF-hand loop and the atomic charges on Ca^{2+}. The charge of the Glu residue at position 12 was less than $-1e$ by ~20% commonly in all four EF-hand loops because in solution, the side chain of the residue at the 12th position is usually in the bidentate coordination mode,[45] and it is expected that more charge transfer occurs

between this residue and the Ca^{2+} ion. For other coordinating residues, i.e., residues at positions 1, 3, 5, 7, and 9, on average, there could be an increase in the magnitude of the negative charges or barely any charge redistribution (close to $-1e$ or 0). Surprisingly, for the residues that are not actively involved in Ca^{2+} coordination, the average amino acid charges also deviate from the default/nominal values, especially for Lys at the second position in EF-1, where charge transfer seems to occur between neighboring Ca^{2+}-coordinating residues, such as the three Asp residues at the first, third, and fifth positions. Furthermore, large standard deviations were observed for all of the amino acid charges on the protein (Fig. S7), which suggests that these charges are systematically dependent on the loop configurations; hence, methodical charge assignment on the protein is required in the MD force field development of Ca^{2+} and amino acids in the protein ion binding site.

E. The conformation of the Ca^{2+} binding loops dictates the number of water molecules coordinating Ca^{2+}

We show that the conformation of the Ca^{2+} binding loops that vary with CaM-binding targets (CaMBTs) dictates the number of water molecules that coordinates Ca^{2+}. To explore the conformational variation of the EF-hand loops in our MD simulations, we plotted (Fig. 8) the potential of mean force (PMF) as a function of the asphericity of the EF-hand (Δ; see the definition in the supplementary material) and the distance from the Ca^{2+} ion to the center of mass (COM) of the corresponding loop (d_{COM}). There are substantial differences in the PMFs between the Ca^{2+}-retaining (Ca^{2+}/CaM or Ca^{2+}/CaM/CaMKII) and Ca^{2+}-releasing (Ca^{2+}/CaM/Ng) environments. In the former, the position of Ca^{2+}
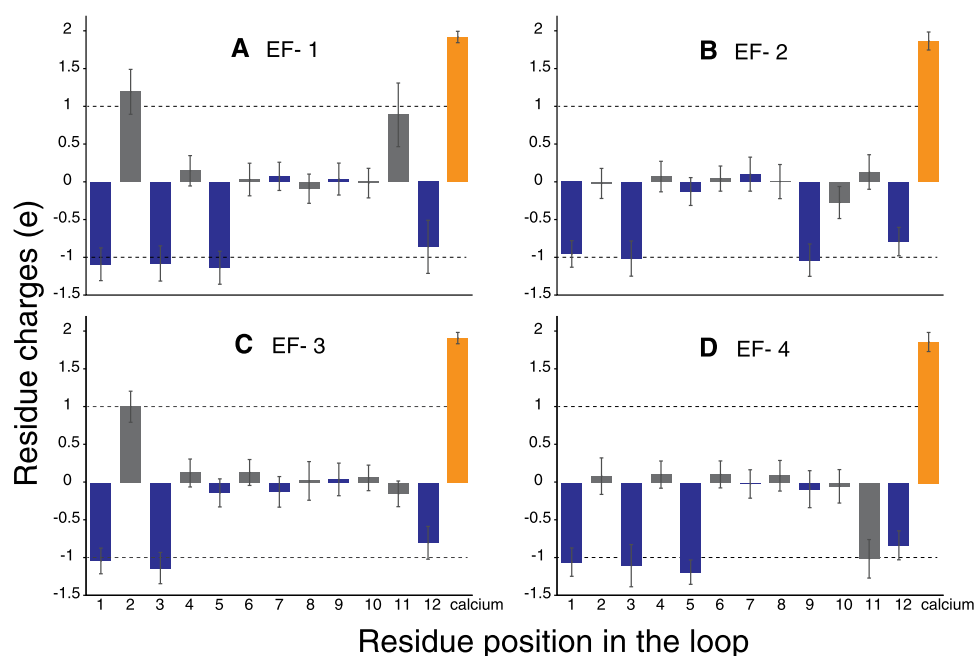

FIG. 7. Average net charges per residue in the EF-hand loops. The i_RESP fitted charges are summed for each residue in each loop. The mean and the standard deviation of the residual charges are shown for the four EF-hand loops (a)–(d). Residues chelating Ca^{2+} in the crystal form of the EF-hand loop in Ca^{2+}/CaM are colored blue, other residues are colored gray, and Ca^{2+} is colored orange.
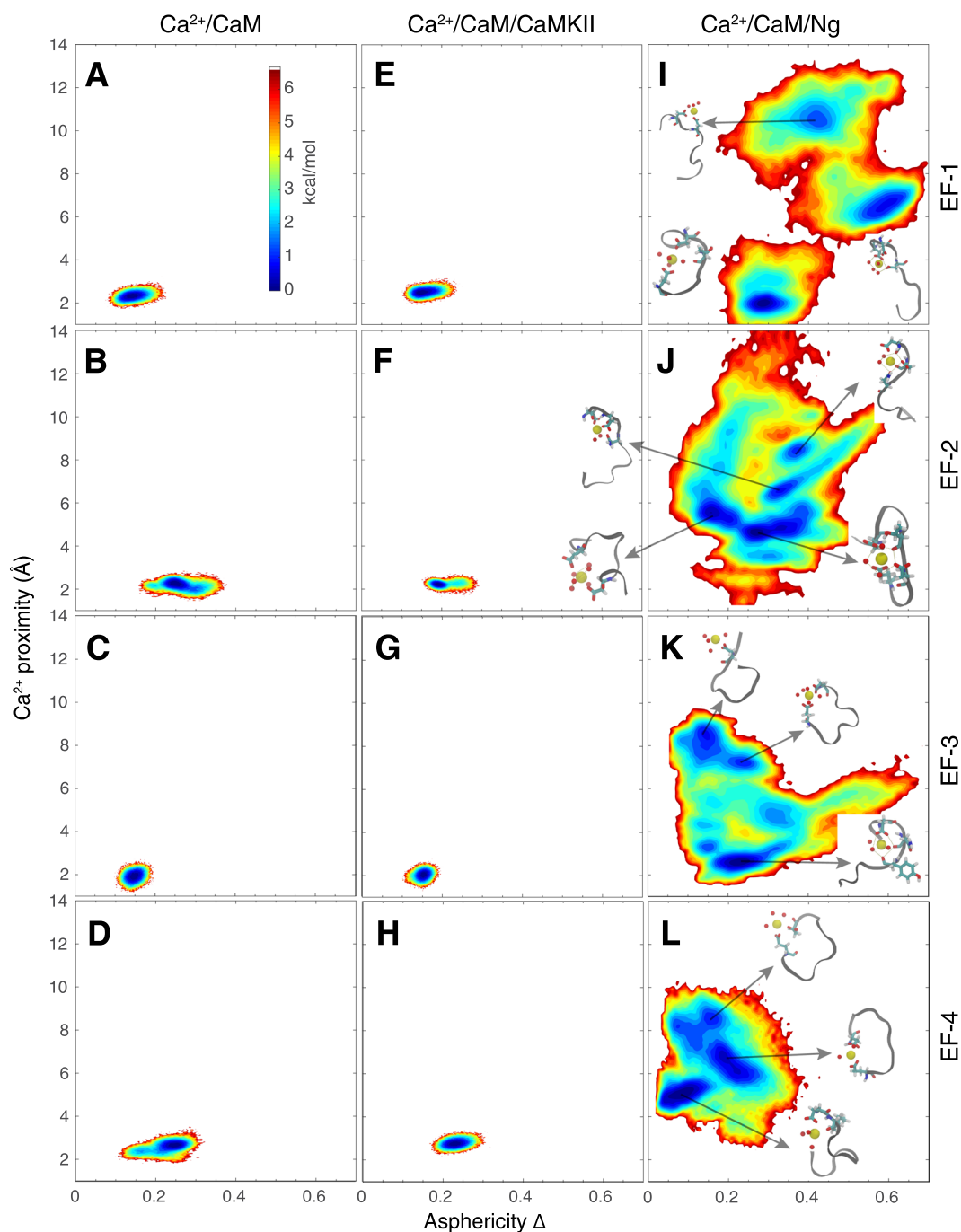
FIG. 8. The potential of the mean force (PMF) as a function of the asphericity (Δ) of the loop and the distance between Ca^{2+} and the center of mass of the loop. The PMFs are plotted for four individual EF-hand loops from three types of sample systems: (a)–(d) Ca^{2+}/CaM, (e)–(h) Ca^{2+}/CaM/CaMKII, and (i)–(l) Ca^{2+}/CaM/Ng. The color bar is scaled by kcal/mol, and the lowest PMF value is set to 0 kcal/mol.

is restricted and close to the center of the loop (d_{COM} = 2–3 Å), as shown in Figs. 8(a)–8(h), and the EF-hand loops are generally spherical with Δ = 0.2–0.3 to promote the holospherical coordination of Ca^{2+} by the EF-hand loop. In the latter, there are several basins along a wide range of both Δ and d_{COM}, as shown in Figs. 8(i)–8(l). d_{COM} varies from 2 Å to as large as 10 Å, which means that Ca^{2+} in the CaM/Ng complex can be bound, loosely bound, or unbound. Δ varies from 0 to 0.6, corresponding to the spherical
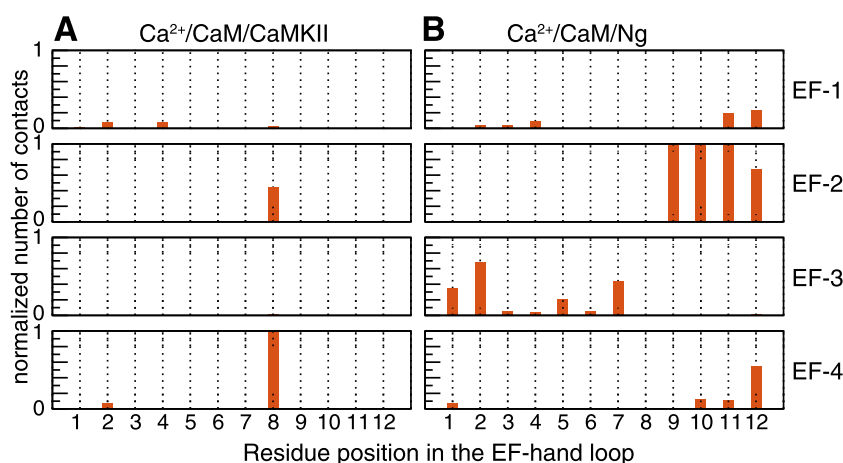
FIG. 9. Contact formation between loops and the target. Snapshots from all-atomistic molecular dynamics simulations of Ca^{2+}/CaM/CaMKII and Ca^{2+}/CaM/Ng. A contact is formed if the distance between any atom from a residue in the loop and any atom from the residues in the CaMBT is within 4 Å. The number of contacts is then normalized by the number of snapshots and corresponding maximum number of contacts in each system.

and largely linear EF-hand loops. The spherical shape of the EF-hand loops mostly corresponds to close proximity of Ca^{2+}, which leads to the bound state of Ca^{2+} in a holospherical coordination geometry. A more linear shape of the EF-hand loops leads to hemispherical or planar geometries of coordination of Ca^{2+} by the EF-hand loops, where nearby water molecules take the place of the protein oxygen atoms and N_{water} increases.

To gain a deeper understanding of the role of the amino acids in the EF-hand loops in determining the Ca^{2+} stability in the EF-hand loops, we investigated the intermolecular interaction between the loop and the CaMBT. The following describes tiers of residues that were found to be involved in these interactions. (i) The residues at positions 1 and 12 coordinate Ca^{2+} most consistently, while other residues are more often substituted by water molecules when Ca^{2+} is loosely bound (Fig. 8). These two residues are rarely involved in the interaction with CaMBT (Fig. 9). (ii) In the crystal structure of CaM, to coordinate Ca^{2+}, the residue at position 7 extends its backbone oxygen toward Ca^{2+}, and the subsequent residue at position 9 moves far away from Ca^{2+}, requiring a water molecule to chelate Ca^{2+}. These "frustrated" residues are dedicated to forming an EF-hand β-scaffold with their counterparts in the neighboring EF-hand loop to stabilize the shape of the two EF-hands in the same lobe of CaM.[8] (iii) Residue 8 is usually hydrophobic and not actively involved in Ca^{2+} coordination. Its backbone is part of the EF-hand β-scaffold, and the direction of the side chain is tuned by CaMBT. When the side chain points toward CaMKII (contacts are found between residue 8 and CaMKII in Fig. 9), Ca^{2+} binding is enhanced; when the side chain points away from Ng (no contact between residue 8 and Ng is observed in Fig. 9), Ca^{2+} binding is weakened.

IV. DISCUSSION

A. Water molecules contribute to the coordination of divalent Ca^{2+} in EF-hand loops

We have established a feasible functional for the quantum mechanical calculation of Ca^{2+} in the EF-hand loops of the CaM protein. With the electronic structures involving all the amino acids in a calcium binding loop and Ca^{2+}, we showed that the geometry of the calcium binding loop is essential in stabilizing the pentagonal bipyramidal coordination of divalent Ca^{2+}. Ca^{2+} is a metal ion that exhibits variability in coordination number and geometry because of its relatively large size, allowing close packing of its ligands.[18,46] Ca^{2+} ions are most commonly coordinated by seven or eight ligands in the crystal form.[47] For the EF-hand loops in a Ca^{2+}-binding protein, the coordination of Ca^{2+} usually presents a pentagonal bipyramidal geometry (Fig. 1). In the crystal structure of CaM, to form the pentagonal geometry, the crucial feature is the conserved 12th residue, which contributes two carboxylate oxygen groups (bidentate) due to its long side chain. Mutating the 12th residue to a shorter side chain, such as Asp, leads to an octagonal geometry and a decrease in Ca^{2+} affinity by 100fold.[47] The bidentate feature has been thought to be the main reason that EF-hands can bind Ca^{2+} with higher affinity over other divalent ions such as Mg^{2+} or Zn^{2+}.[47]

For the two apexes in the bipyramidal geometry, a water molecule is necessary as a bridge between the Ca^{2+} and a side chain that remains too far away either because of the limited length of the side chain or to fulfill its active role in other functions. Regarding the latter reason, one example is the ninth residue belonging to the β-sheet structure between two EF-hand loops in a lobe of CaM, which is termed the EF-hand β-scaffold.[48] Interactions between this residue and the other loop, with or without interactions with CaMBT, can affect the stability and conformation of the EF-hand loop, which further influences the Ca^{2+} coordination geometry.[8] Due to the mobility of the water molecules, the pentagonal bipyramidal geometry can be easily converted to six-coordinate (octagonal geometry) or eight-coordinate, where two water molecules are observed as in the crystal structures.[47]

In our MD simulations, we show that packing two water molecules around the Ca^{2+} ion is of the highest probability (Fig. 5). This agrees with the classical MD simulations of Ca^{2+} in an EF-hand loop without polarization effects.[49] For the Ca^{2+}-retaining environment, the water molecules surrounding the Ca^{2+} ion allow for flexibility in the protein dynamics while retaining Ca^{2+} in the pentagonal bipyramidal geometry. For the Ca^{2+}-releasing

environment Ca^{2+}/CaM/Ng, there are three to six water molecules in the first solvation shell. Ca^{2+} ions are likely to be partially or completely exposed to the solvent and partially coordinated by EF-hand loops [Figs. 8(i)–8(l)]. This also suggests that the coordination geometry of Ca^{2+} involving at least one water molecule dynamically responds to changes in the local environment, which could be the result of binding or dissociation of a CaM binding target.

B. Determining the atomic charge of Ca^{2+} requires information on the loop geometry

For divalent ions such as Ca^{2+}, force field development has been limited to bare ions in aqueous solution.[10] To address the force field of Ca^{2+} in protein environments, Jungwirth's group accounted for the effective polarization[9] by scaling the ionic charges by a factor of 0.75 in a classical force field. In this case, the computed value of the affinity of Ca^{2+} in the four individual EF-hands of CaM is approximately twice the experimentally measured values.[50] This mean-field approach does not determine charge distribution on the protein directly, which impacts the shape of the EF-hand loop and the affinity and dynamics of Ca^{2+} binding. An ensemble average approach was adopted by Cheung et al.,[8,51] that averages an ensemble of semiempirically determined atomic charges obtained from an ensemble of protein configurations involving the loops, where the Ca^{2+} atomic charge ranges from +1.2 to +1.8e. However, the polarization effect was not explicitly included.

To fix the correct coordination geometry, multi-site models for divalent ions have been developed by including multiple fixed or constrained dummy cations around the divalent ion center.[52–54] However, since different coordination geometries for Ca^{2+} are observed in experimental solved structures of Ca^{2+} binding proteins,[55] it is expected that the coordination geometry changes when the binding site is conformationally flexible, especially during association/dissociation of Ca^{2+}. Those multi-site models are incapable of capturing the change in the coordination geometry.

According to the work performed by Jing et al.,[11] many-body effects play an essential role in correctly determining the Ca^{2+} affinity. In this work, we show that there is nonuniform charge redistribution across all residues in the EF-hand loop in Fig. 7, meaning that their interactions with Ca^{2+} cannot be simplified by considering only a few amino acids from the entire loop. Therefore, we allow all possible coordination geometries around the ion by including all the residues in the loop and the coordinating water with Ca^{2+} in the ESP calculation.

According to our collected EF-hand loop geometries, we showed that RESP charges vary from 1.5 to 1.9e, and this is consistent with the charge values by the aforementioned studies by Jungwirth, where polarization effects were effectively included by scaling down the Ca^{2+} charge (2e) as used in popular MD force fields. In contrast, for the i_RESP charges, which are applicable to AMBER polarizable force fields where the polarization effect is explicitly included, the values vary in the range of 1.2 to 2.4e.

C. Ionic radius of Ca^{2+} in the electrostatic potential calculation

In this work, we compared the atomic charges fitted to ESPs generated using several ionic radii of Ca^{2+}. In order to determine

the grid for ESP calculation at the quantum level, we first explored vdW radii of Ca^{2+} ions from MD force fields. We noticed that there were discrepancies between the vdW radii of Ca^{2+} ions in the Lennard-Jones potential in popular nonpolarizable force fields. In the AMBER, CHARMM/27, and OPLS-AA force fields, 1.7 Å is used; in GROMOS, ~2.0 Å is used; in CHARMM/36, 1.37 Å is used. Controversial results were found for all those values in the calculation of the hydration free energy or binding affinity.[8,49,56–58] The discrepancies do not necessarily imply that the current vdW parameters of Ca^{2+} in those nonpolarizable force fields are unreasonable since those ion parameters were developed to reproduce molecular properties such as hydration free energy and coordination numbers in aqueous solution. Moreover, we cannot separate the radius and well-depth when determining the VDW parameters. However, these vdW radii for Ca^{2+} are found inappropriate for the calculation of ESPs of the Ca^{2+} binding proteins at the quantum mechanical level. We showed that a value of 1.7 Å failed to generate physical atomic charges for Ca^{2+} for some geometries, and the result did not improve by performing energy minimization before the QM calculation. In more detail, as shown in Fig. S8 of the supplementary material, the distribution of the Ca^{2+} i_RESP partial charges from QM energy minimized structures is wide and similar to the distribution of charges obtained directly using the MD structures. Those geometries extracted from the MD trajectories are stabilized by using the vdW parameters from the MD force field; however, in the QM calculation, the Ca^{2+} radius is improperly large to cause artifacts, especially when the coordinating water molecules are explicitly included. Nevertheless, a large radius of 2.28 Å was adopted to account for the solvation effects when the COnductor-like Screening MOdel (COSMO) implicit water model was used.[59] We suggest that small ionic radii for Ca^{2+} and other divalent ions should be used in the RESP/i_RESP charge fitting when the solvent molecules are explicitly included.

V. CONCLUSIONS

CaM senses a broad spectrum of oscillatory Ca^{2+} signals for eukaryotic cells and acts as a hub for many downstream pathways.[2,60] From incoming calcium signals to a particular pathway, an additional peptide (i.e., CaMBT) is required for tuning CaM's response.[61] Specific regions in CaMBT can tune the Ca^{2+} binding affinity for the EF-hand loop by stabilizing or disrupting interactions with the EF-hand loop.[8] Because of such conformational flexibility in the EF-hand loop and dynamically adapting coordination geometries of the Ca^{2+} ions, we developed an approach of deriving conformational dependent atomic charges that is based on QM calculations including all the residues in the EF-hand loop.

Applying the approach to snapshots of Ca^{2+} in an EF-hand loop from MD simulations of CaM and a couple of CaMBTs, we show that in response to the dynamic coordination geometry of Ca^{2+}, the atomic charge of Ca^{2+} alters and follows a Gaussian-like distribution. However, the underlying connection between the Ca^{2+} charge and the structure of the Ca^{2+} binding site as well as the coordination geometry is elusive. We will use machine learning methods to address this connection and implement a model into a MD package in our future study.

Our approach can be applied to Ca^{2+} in other protein environments and other divalent ions for advancing the development of

both nonpolarizable and polarizable force fields for divalent ions in dynamic environments.

SUPPLEMENTARY MATERIAL

See the supplementary material for the initial structures of the complex of the Ca^{2+}/CaM and Ng peptide, representative EF-hand loop structures including the derived Ca^{2+} charges, and additional details about the settings, parameters, and discussion about the charge derivation.

ACKNOWLEDGMENTS

DATA AVAILABILITY

The data that support the findings of this study are available within the article and its supplementary material. The EF-hand loop structures and derived charge data are available from the corresponding author upon reasonable request.

REFERENCES

[1]M. N. Waxham and M. S. Cheung, in *Encyclopedia of Computational Neuroscience*, edited by D. Jaeger and R. Jung (Springer, 2013).
[2]A. P. Yamniuk and H. J. Vogel, Mol. Biotechnol. **27**, 33 (2004).
[3]Z. Xia and D. R. Storm, Nat. Rev. Neurosci. **6**, 267 (2005).
[4]H. Tidow and P. Nissen, FEBS J. **280**, 5551 (2013).
[5]G. C. Faas, S. Raghavachari, J. E. Lisman, and I. Mody, Nat. Neurosci. **14**, 301 (2011).
[6]L. Hoffman, A. Chandrasekar, X. Wang, J. A. Putkey, and M. N. Waxham, J. Biol. Chem. **289**, 14644 (2014).
[7]J. B. Foresman and Æ. Frisch, *Exploring Chemistry with Electronic Structure Methods*, 2nd ed. (Gaussian Inc., Wallingford, CT, 1995), p. 122.
[8]P. Zhang, S. Tripathi, H. Trinh, and M. S. Cheung, Biophys. J. **112**, 1105 (2017).
[9]I. Leontyev and A. Stuchebrukhov, Phys. Chem. Chem. Phys. **13**, 2613 (2011).
[10]D. Jiao, C. King, A. Grossfield, T. A. Darden, and P. Ren, J. Phys. Chem. B **110**, 18553 (2006).
[11]Z. Jing, C. Liu, R. Qi, and P. Ren, Proc. Natl. Acad. Sci. U. S. A. **115**, E7495 (2018).
[12]J. Melcr and J. P. Piquemal, Front. Mol. Biosci. **6**, 143 (2019).
[13]C. Kobayashi and S. Takada, Biophys. J. **90**, 3043 (2006).
[14]T. Ikeda, M. Boero, and K. Terakura, J. Chem. Phys. **127**, 074503 (2007).
[15]M. Ikura, Trends Biochem. Sci. **21**, 14 (1996).
[16]M. R. Nelson and W. J. Chazin, Protein Sci. **7**, 270 (1998).
[17]M. M. Harding, Acta Crystallogr., Sect. D: Biol. Crystallogr. **55**, 1432 (1999).
[18]T. Dudev and C. Lim, Chem. Rev. **103**, 773 (2003).
[19]C. I. Bayly, P. Cieplak, W. Cornell, and P. A. Kollman, J. Phys. Chem. **97**, 10269 (1993).
[20]P. Cieplak, W. D. Cornell, C. Bayly, and P. A. Kollman, J. Comput. Chem. **16**, 1357 (1995).
[21]O. Borodin, J. Phys. Chem. B **113**, 11463 (2009).
[22]K. Schulten and M. Tesch, Chem. Phys. **158**, 421 (1991).
[23]J. B. Hooper, O. N. Starovoytov, O. Borodin, D. Bedrov, and G. D. Smith, J. Chem. Phys. **136**, 194506 (2012).
[24]O. N. Starovoytov, H. Torabifard, and G. A. Cisneros, J. Phys. Chem. B **118**, 7156 (2014).
[25]R. E. Duke, O. N. Starovoytov, J.-P. Piquemal, and G. A. Cisneros, J. Chem. Theory Comput. **10**, 1361 (2014).
[26]H. Torabifard, O. N. Starovoytov, P. Ren, and G. A. Cisneros, Theor. Chem. Acc. **134**, 101 (2015).
[27]M. J. Abraham, T. Murtola, R. Schulz, S. Páll, J. C. Smith, B. Hess, and E. Lindahl, SoftwareX **1-2**, 19 (2015).
[28]W. L. Jorgensen, J. Chandrasekhar, J. D. Madura, R. W. Impey, and M. L. Klein, J. Chem. Phys. **79**, 926 (1983).
[29]B. Hess, H. Bekker, H. J. C. Berendsen, and J. G. E. M. Fraaije, J. Comput. Chem. **18**, 1463 (1997).
[30]K. Lindorff-Larsen, S. Piana, K. Palmo, P. Maragakis, J. L. Klepeis, R. O. Dror, and D. E. Shaw, Proteins **78**, 1950 (2010).
[31]T. Darden, D. York, and L. Pedersen, J. Chem. Phys. **98**, 10089 (1993).
[32]M. Parrinello and A. Rahman, J. Appl. Phys. **52**, 7182 (1981).
[33]Z. Guo and D. Thirumalai, Folding Des. **2**, 377 (1997).
[34]B. K. Rai and G. A. Bakken, J. Comput. Chem. **34**, 1661 (2013).
[35]J. Behler, J. Chem. Phys. **145**, 170901 (2016).
[36]M. J. Frisch, G. W. Trucks, H. B. Schlegel, G. E. Scuseria, M. A. Robb, J. R. Cheeseman, G. Scalmani, V. Barone, G. A. Petersson, H. Nakatsuji, X. Li, M. Caricato, A. V. Marenich, J. Bloino, B. G. Janesko, R. Gomperts, B. Mennucci, H. P. Hratchian, J. V. Ortiz, A. F. Izmaylov, J. L. Sonnenberg, D. Williams, F. Ding, F. Lipparini, F. Egidi, J. Goings, B. Peng, A. Petrone, T. Henderson, D. Ranasinghe, V. G. Zakrzewski, J. Gao, N. Rega, G. Zheng, W. Liang, M. Hada, M. Ehara, K. Toyota, R. Fukuda, J. Hasegawa, M. Ishida, T. Nakajima, Y. Honda, O. Kitao, H. Nakai, T. Vreven, K. Throssell, J. A. Montgomery, Jr., J. E. Peralta, F. Ogliaro, M. J. Bearpark, J. J. Heyd, E. N. Brothers, K. N. Kudin, V. N. Staroverov, T. A. Keith, R. Kobayashi, J. Normand, K. Raghavachari, A. P. Rendell, J. C. Burant, S. S. Iyengar, J. Tomasi, M. Cossi, J. M. Millam, M. Klene, C. Adamo, R. Cammi, J. W. Ochterski, R. L. Martin, K. Morokuma, O. Farkas, J. B. Foresman, and D. J. Fox, Gaussian 16, Rev. C.01, Gaussian Inc., Wallingford, CT, 2016.
[37]P. Cieplak, J. Caldwell, and P. Kollman, J. Comput. Chem. **22**, 1048 (2001).
[38]J. W. Caldwell and P. A. Kollman, J. Phys. Chem. **99**, 6208 (1995).
[39]U. Öpik, Proc. Phys. Soc **92**, 566 (1967).
[40]J. Wang, P. Cieplak, J. Li, J. Wang, Q. Cai, M. Hsieh, H. Lei, R. Luo, and Y. Duan, J. Phys. Chem. B **115**, 3100 (2011).
[41]A. D. Becke, J. Chem. Phys. **98**, 5648 (1993).
[42]A. Schäfer, H. Horn, and R. Ahlrichs, J. Chem. Phys. **97**, 2571 (1992).
[43]J. Åqvist, J. Phys. Chem. **94**, 8021 (1990).
[44]R. D. Shannon, Acta Crystallogr., Sect. A **32**, 751 (1976).
[45]M. Nara, H. Morii, and M. Tanokura, Biochim. Biophys. Acta **1828**, 2319 (2013).
[46]J. J. Falke, S. K. Drake, A. L. Hazard, and O. B. Peersen, Q. Rev. Biophys. **27**, 219 (1994).
[47]A. K. Katz, J. P. Glusker, S. A. Beebe, and C. W. Bock, J. Am. Chem. Soc. **118**, 5752 (1996).
[48]Z. Grabarek, J. Mol. Biol. **359**, 509 (2006).
[49]S. Marchand and B. Roux, Proteins **33**, 265 (1998).
[50]M. Kohagen, M. Lepšík, and P. Jungwirth, J. Phys. Chem. Lett. **5**, 3964 (2014).
[51]Q. Wang, P. Zhang, L. Hoffman, S. Tripathi, D. Homouz, Y. Liu, M. N. Waxham, and M. S. Cheung, Proc. Natl. Acad. Sci. U. S. A. **110**, 20545 (2013).
[52]P. Oelschlaeger, M. Klahn, W. A. Beard, S. H. Wilson, and A. Warshel, J. Mol. Biol. **366**, 687 (2007).
[53]J. Aaqvist and A. Warshel, J. Am. Chem. Soc. **112**, 2860 (1990).
[54]A. Saxena and D. Sept, J. Chem. Theory Comput. **9**, 3538 (2013).
[55]E. Pidcock and G. R. Moore, J. Biol. Inorg. Chem. **6**, 479 (2001).

[56] C. Chen, Y. Huang, X. Jiang, and Y. Xiao, Phys. Rev. E **87**, 062705 (2013).

[57] A. Basit, R. K. Mishra, and P. Bandyopadhyay, "Calcium ion binding to calmodulin: binding free energy calculation using the molecular mechanics Poisson-Boltzmann surface area (MM-PBSA) method by incorporating implicit polarization," J. Biomol. Struct. Dyn. (published online).

[58] M. Lawrenz, J. Wereszczynski, R. Amaro, R. Walker, A. Roitberg, and J. A. McCammon, Proteins **78**, 2523 (2010).

[59] M. Lepsik and M. J. Field, J. Phys. Chem. B **111**, 10012 (2007).

[60] K. P. Hoeflich and M. Ikura, Cell **108**, 739 (2002).

[61] Y. Kubota, J. A. Putkey, and M. N. Waxham, Biophys. J. **93**, 3848 (2007).